ICAS 2021 SHANGHAI
International Council of the Aeronautical Sciences
32nd Congress of the International Council of the Aeronautical Sciences
September 6-10, 2021
Pudong Shangri-La, Shanghai, China

VALIDATION OF AN AERODYNAMIC MODEL FOR THE ANALYSIS OF SUBSCALE TEST AIRCRAFT WITH DISTRIBUTED ELECTRICAL PROPULSION

Oliver Luderer[1], Marc Jünemann[1] & Frank Thielecke[1]

[1]Hamburg University of Technology , Institute of Aircraft Systems Engineering , Nesspriel 5, 21129 Hamburg, Germany

Abstract

In this publication an aerodynamic model for the estimation of aerodynamic effects of propeller-wing-interaction for analysis, design and construction of subscale test aircraft (STA) is presented. The well-established programmes XFOIL, XROTOR and LIFTING_LINE are used as subroutines in an automated analysis process. The model for propeller-induced velocities is based on a combination of blade-element theory and a vortex theory. The effect of propeller slipstream contraction on the simplified velocity field is considered with a semi-empirical model. To estimate the spanwise lift distribution of the wing, a multi-lifting line method was chosen which accounts for the additional axial and transverse slipstream velocities. Comparison of simulation results with measurement data from wind tunnel tests shows satisfying accuracies regarding thrust, wing polars, and spanwise lift distribution. In addition, the toolchain is integrated into a modular software framework for design and construction of SubsCALe test AircRaft (SCALAR). Its application is exemplified with a resizing study of a subscale aicraft model with distributed electrical propulsion. The study shows that the overall impact on the layout of the subscale test aircraft is of minor importance. Nonetheless, it is outlined that the presented aerodynamic toolchain serves well as a basis for mission-dependent wing load estimation in planned technology demonstration campaigns.

Keywords: Distributed propulsion, Propeller-wing-interaction, Subscale test aircraft, Preliminary Design

1. Introduction

The use of down-scaled aircraft as flying testbeds is regarded as a promising low-risk solution for early demonstration and assessment of innovative technologies [1]. To rapidly analyze, manufacture, and fly a subscale test aircraft (STA), a coherent aircraft layout for the scaled size of the demonstrator has to be designed. At the Institute of Aircraft Systems Engineering (FST) of Hamburg University of Technology (TUHH) the sizing and synthesis process for an STA is based on a classical conceptual design approach [2]. To this end, well-known sizing methods and analysis tools for design disciplines like aerodynamics, structures, flight mechanics, and on-board systems are used in an iterative aircraft design process. These methods are complemented by practical knowledge patterns gained from long-year experience in design and construction of STAs. For the analysis of STAs with distributed electrical propulsion (DEP), however, the implemented methods are incomplete, because they do not represent aerodynamic interaction between propeller and wing. It is especially important to account for these effects, if technologies for load sensing and alleviation systems are analyzed. In this case, a concurrent development of computational models for load estimation and the physical testbed is necessary to optimize the architecture of complementary sensors, and define strategies for data fusion and load control. In this paper, an automated process for model-based estimation of spanwise lift distribution during conceptual stage is presented, which accounts for the aerodynamic interactions. Methods for the analysis of 2D-airfoil and propeller aerodynamics, propeller slipstream contraction, and spanwise wing lift distribution are combined in an automated toolchain. To this end, the well-established aerodynamic analysis programmes XFOIL, XROTOR, and LIFTING_LINE are used. To validate the toolchain, simulation results are compared with experimental data from wind

tunnel tests of existing propeller and wing components of STAs.

The paper is structured as follows: The implemented aerodynamic models are described in Sec. 2. In Sec. 3.the experimental set-up of the wind tunnel tests and design of experiments are depicted. A validation of the implemented analysis process by comparing simulation results and data from wind tunnel tests is presented in Sec. 4. In Sec. 5. the process is exemplified by an integration into a modular software framework for design and construction of SubsCALe test AircRaft (SCALAR) and its application for a resizing study of a subscale aircraft model with distributed electrical propulsion (DEP). As an outlook, the prospective use of the presented toolchain for subscale technology verification of load sensing and alleviation systems is discussed.

2. Aerodynamic Model for Propeller-Wing-Interaction

The process to analyze the spanwise lift distribution of a wing having distributed propellers along the leading edge is based on already existing implementations of aerodynamic analysis models for 2D profiles, propeller plane and slipstream velocities, and wing lift. These tools were validated and are well accepted by the aircraft conceptual design community. In Fig. 1, the consecutive process is depicted. First, lift and drag characteristics of 2D profiles of propeller blades and lifting surfaces are analyzed with XFOIL. In a second step, axial and transverse velocities induced by the propellers are analyzed using XROTOR. The effect of slipstream contraction on the induced velocities is estimated using a semi-empirical slipstream model. A multi-lifting line method in LIFTING_LINE is used for the analysis of wing aerodynamics. Used models and underlying assumption of the four steps are outlined in the following sections.

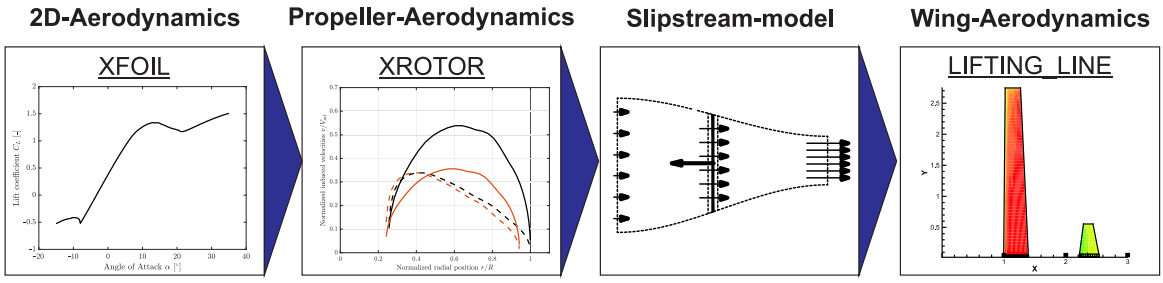

Figure 1 – Propeller-Wing-Interaction Toolchain

2.1 Airfoil characteristics

For the 2D aerodynamics analysis of the wing and propeller blade profiles the panel code XFOIL [3, 4] was chosen. Due to the different background disturbance levels of propeller blade area and wing plane, different settings of the transition parameter N_{crit} for the e^n method to predict flow transition have to be selected in XFOIL. While the default e^9 amplification is used for wing profile analysis, this parameter was changed for blade profile analysis to describe a fully turbulent flow. In Tab. 1, the selection of transition parameters (e.g. transition points) are summarized. The considered range of angle of attack for propeller airfoil analysis is selected such that the upper and lower stall boundaries of the airfoil polars are covered. The input parameter for Mach number is set to zero, because a Mach number correction is applied in XROTOR itself. The respective Reynolds number depends on the operating point, which results in an individual Reynolds number for each radial position r, rotational speed Ω and variation of the free stream velocity $V_{\inf}$ at constant ambient temperature.

Table 1 – XFOIL properties for propeller analyses

Fully turbulent flow:	$N_{crit} = 0.01$	Angle of attack interval:	$\alpha = -15° : 0.25° : 40°$
Upper transition point:	$XtrTop = 1$	Mach number:	$Ma = 0$
Lower transition point:	$XtrBot = 1$	Reynolds number:	$Re = f(\, r, V_{\inf}, \Omega \,)$
Panel discretization:	$n_{panels} = 200$		

Subsequently, the resulting two-dimensional airfoil polars are corrected for effects of rotating propeller blades. As reported by Himmelskamp [5] and Snel [6] the rotation of propeller blades leads to a stall delay, which significantly increases the maximum lift coefficient compared to static two-dimensional analyses. This effect can be approximated using empirical models as it was shown for example by Snel [6] or Du and Selig [7]. In this publication, an extended correction model for UAV applications at low Reynolds numbers according to MacNeill [8] is applied (cf. Eq. 1).

$$C_{L,2D,corr} = C_{L,2D} + \frac{r}{R} \cdot \tanh\left(3.1 \cdot \left(\frac{\Omega \cdot c}{V_{eff}}\right)^2\right) \cdot (C_{L,linear} - C_{L,2D}) \tag{1}$$

2.2 Propeller model

The propeller aerodynamics are based on the propeller model XROTOR developed by Drela and Youngren [9]. XROTOR combines a blade-element theory with three selectable options for the calculation of propeller induced velocities. In a previous study by Lemke et al. [10], results indicate that the prediction of radial velocity distribution and amplitudes is decisive for the accuracy of the overall model for propeller-wing-interaction, because the propeller-induced axial- and tangential velocities have major impact on dynamic pressure and effective angle of attack of the wing. A vortex-theory approach for velocity estimation is used in this publication, because it has the most expected prediction accuracy. Necessary inputs for XROTOR are the propeller geometry, which is derived by 3D scans of the propeller-blade, and the 2D lift and drag characteristics of the blade airfoils, which are analyzed by XFOIL. The results of XROTOR are limited to flow conditions at $\alpha = 0°$ and $\beta = 0°$.

2.3 Slipstream model

The slipstream model used in this paper is a combination of the slipstream contraction model by Smelt and Davies [11] and an approach to account for change in axial induced velocity due to the slipstream contraction by Patterson [12]. According to Smelt and Davies, the contracted propeller slipstream diameter $D_{contr}(x)$ can be described by

$$D_{contr}(x) = D \cdot \sqrt{\frac{1+a}{1+a \cdot \left(1 + \frac{x}{\sqrt{x^2 + D^2/4}}\right)}} \tag{2}$$

where D is the propeller diameter, x is the distance from the propeller plane, and a the axial induction factor. The induction factor a is calculated from the induced mean axial velocity in the propeller plane $\bar{v}_{ax}$ and the free stream velocity $V_{\inf}$.

$$a = \frac{\bar{v}_{ax}}{V_{\inf}} \tag{3}$$

According to Patterson, the axial induced propeller velocities $v_{ax}(r/R)$ acting on the wing in a tractor configuration depends on the operating point and geometric characteristics of propeller and wing (position, radius, wing chord). He shows that a multiplication factor of $\beta < 1$ might result, if propellers with small diameters compared to the wing chord are installed. This case is relevant for the target aircraft configuration as discussed in Sec. 5.1. It leads to a reduced axial induced velocity at the trailing edge of the wing. This correction of the axial induced velocity of an installed propeller is modeled by Eq. 4 (cf. [12]).

$$v_{ax,corr}(r/R) = \beta \cdot v_{ax}(r/R) \tag{4}$$

2.4 Wing aerodynamics

The multi-lifting-line method LIFTING_LINE [13] developed by the German Aerospace Center (DLR) is applied to analyze the spanwise lift distribution. In essence, the model uses an enhanced vortex lattice method (VLM) where the circulation distribution of each vortex is assumed to be a quadratic

function in spanwise direction. The total lift coefficient of the wing and the local lift coefficients of dedicated elementary wings are calculated normalized to the wing area S_{ref} and the dynamic pressure $q_{\inf} = \rho/2 \cdot V_{\inf}^2$. The model accounts for propeller-induced velocities during the determination of the circulation distribution. Herein, the free stream velocity is superpositioned by the propeller-induced velocities according to Eq. 5.

$$\vec{v}(x,y,z) = \vec{v}_0 + \vec{v}_{Prop}(x,y,z) \tag{5}$$

The following assumptions and limitations apply to LIFTING_LINE:

- incompressible, non-viscous, rotation-free, and stationary flow
- small angles of attack and sideslip angles
- thin airfoils

3. Set-up of Wind Tunnel Tests

Two test rigs were installed in the wind tunnel of Hamburg University of Technology (TUHH) for the experimental validation campaign. The first test rig (PROPA,cf. Fig. 2b) was designed for laboratory and wind tunnel measurements of propeller thrust and torque by making use of calibrated load cells by HBM. During the tests the propeller rotational speed is controlled to constant levels. The second test rig (TETRIS, cf. Fig. 2a) was designed to study the effect of propeller-wing-interactions of STAs. The modular design of TETRIS enables a high degree of flexibility regarding the arrangement of the components. As a result, different motor positions and motor configurations can be examined in the wind tunnel. Although a maximum of three propeller modules are supported, a single motor configuration is used in this paper for model validation in Sec. 4. The modular concept of TETRIS is described by Lemke [10] in more detail. For the tests, 60 local pressure measurements can be acquired in pressure measurement modules at various spanwise positions. The local lift distribution of the area around the central motor of the wing was calculated by integrating the local dynamic pressure measurements of the pressure modules and normalizing the values to the wing chord. Overall forces are measured by use of the wind tunnel balance. The characteristics of the wing segment are shown in Tab. 2. The propeller profiles at varying radial positions were determined by 3D scans. They are required to create the parametric propeller model in XROTOR. Based on preliminary thrust convergence studies with a varying number of profile sections the scanned propellers were broken down into 9 radial profile sections which are shown in Fig. 3a and Fig. 3b. Note, that the related propeller incidence angles are not indicated in the illustrations.

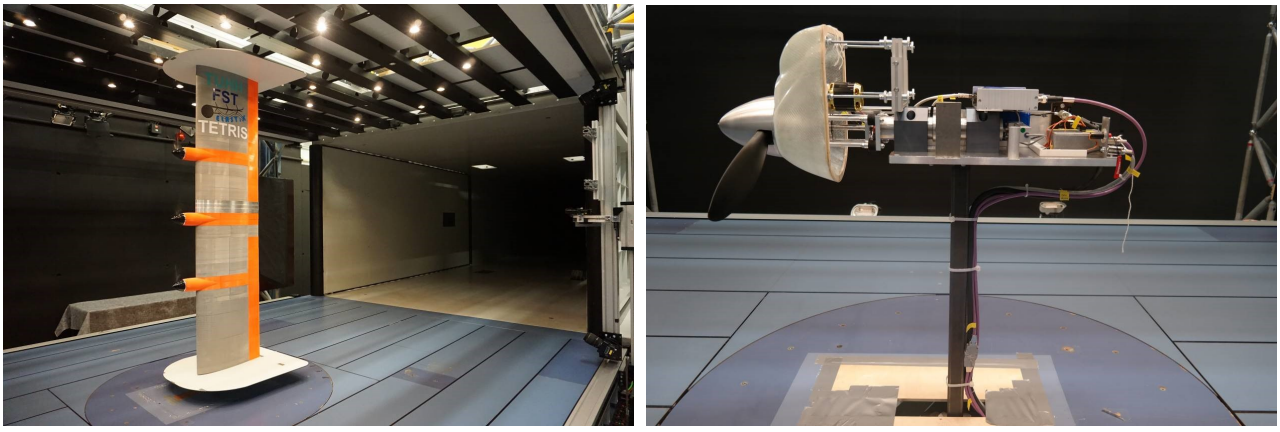

(a) Modular test wing segment - TETRIS (b) Propeller test rig - PROPA

Figure 2 – Test rigs for the wind tunnel experiments

(a) Propeller for TETRIS (b) Propeller for PROPA

Figure 3 – Radial 3D profile scans of the used propellers

Table 2 – TETRIS wing characteristics

Profile	**Wing span** b [m]	**Wing chord** c_w [m]
HQ/W-3/12	1.8	0.46

The design of experiments is summarized in Tab. 3. The validation is subdivided into the analysis of propeller model (PM) and overall propeller-wing-interaction model (PWIM). The PM refers to the combined process of 2D blade profile analysis with XFOIL, XROTOR's analysis of the propeller plane flow, and the slipstream contraction analysis. The combination of PM and LIFTING_LINE builds the overall PWIM. Wind tunnel tests for the validation of the PM are solely focused on thrust measurements at varying free stream velocities. Comparison of the PWIM to wind tunnel data is based on pressure measurements of TETRIS at angles of attack between $-3°$ and $6°$ and a free stream velocity of $V_{\text{inf}} = 16\ \text{m}\,\text{s}^{-1}$.

Table 3 – Test configurations

	TETRIS		PROPA	
Test case	PM	PWIM	PM	PWIM
Angle of attack α [°]	0	-3:3:6	0	-
Sideslip Angle β [°]	0	0	0	-
Free stream velocity V_{inf} [$\text{m}\,\text{s}^{-1}$]	$5:2.5:27.5$	16	$5:5:30$	-
Rotational speed n [min^{-1}]	4000 - 8000	6350, 7700	1300 - 5000	-

4. Model Validation

Before the results of the PWIM are validated against data on the overall and local aerodynamic forces measured during the TETRIS test campaign, the PM is verified and compared to thrust measurements of TETRIS and PROPA in the following.

4.1 Propeller model

As a first verification, simulation results obtained with the propeller model (PM) for the TETRIS and PROPA propeller configurations are shown in Fig. 4. Hereby, the analysis results with and without the effect of the slipstream contraction on the velocities behind a certain distance to the propeller plane are presented. For both analyses the distance from the propeller plane to a supposed wing leading edge is assumed to be $x = 0.075$ m. As can be seen from Fig. 4a, the axial velocity at the wing leading edge for the TETRIS propeller configuration at typical operating conditions ($n = 7700$ min^{-1} and $V_{\text{inf}} = 16\ \text{m}\,\text{s}^{-1}$) is reduced by a factor of 0.73 and the slipstream diameter contracts to $r/R = 0.97$. A similar influence of the slipstream model on the axial and tangential velocities when using the PROPA propeller configuration can be observed in Fig. 4b. Although the results of the

simulation models indicate an expected model behavior, the results can not be validated due to missing measurement data of slipstream velocities.

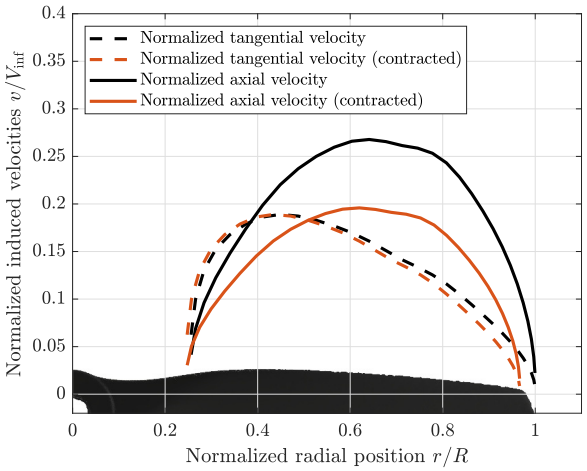

(a) TETRIS propeller configuration at $n = 7700$ min^{-1} and $V_{\inf} = 16\ \mathrm{m\,s}^{-1}$

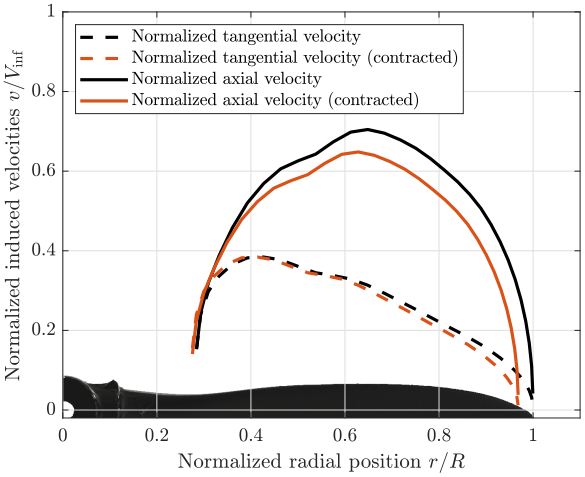

(b) PROPA propeller configuration at $n = 5000$ min^{-1} and $V_{\inf} = 15\ \mathrm{m\,s}^{-1}$

Figure 4 – Axial and tangential induced propeller velocities

Because the thrust of the propeller could not directly be measured during the TETRIS test campaign, it was calculated based on reproducible wind tunnel measurements with a clean wing configuration and a single-motor configuration. By subtracting the wing drag D_{clean} from the measured net thrust T_{net} the gross thrust T_{gross} generated by an isolated propeller can be obtained.

$$T_{gross} = T_{net} - D_{clean} \tag{6}$$

Additional drag due to the propeller slipstream can not be captured here and may lead to small deviations between simulation and measurement. In Fig. 5a, the simulation results of the TETRIS propeller configuration are compared to wind tunnel data. Tolerance bands of 5% and 10% relative deviations to the maximum measured thrust corresponding to 0.7 N and 1.4 N, respectively, indicate the accuracy of the simulations. In general, a good agreement between simulation results of the propeller model and wind tunnel measurement data can be seen. The propeller model slightly overestimates the thrust, especially in the lower thrust region. A maximum deviation of 0.79 N can be observed. The mean absolute deviation from the ideal value is only 0.285 N. No point violates the 10% tolerance band. Only one point violates the 5% tolerance band.

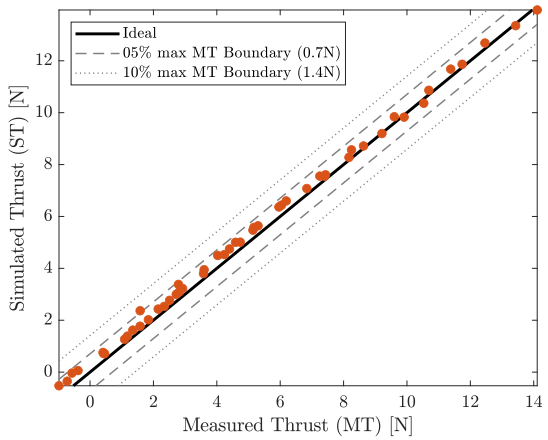

(a) TETRIS propeller configuration

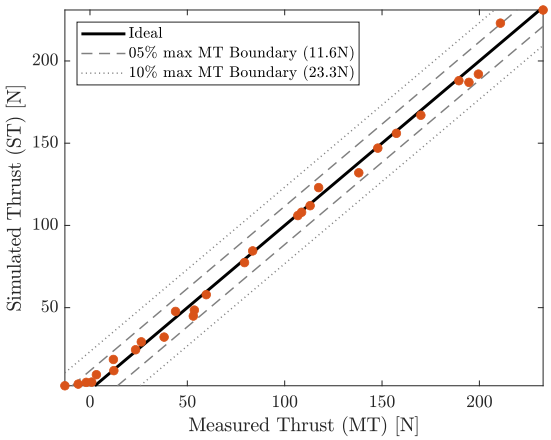

(b) PROPA propeller configuration

Figure 5 – Thrust correlation plots

The results of the simulation model of the PROPA configuration with wind tunnel data are shown in Fig. 5b. The mean absolute deviation from the ideal value is higher compared to TETRIS (4.47 N). While the TETRIS propeller has constant pitch, the pitch of the PROPA propeller is adjustable. This may lead to inaccuracies in the determination of the actual pitch angle due to unintended altering during the installation at the wind tunnel facilities. In addition, the 3D scans of the propeller blade radial profiles revealed a poorer quality compared to the TETRIS propeller scans. This complicated the determination of the 2D shape of the profile sections leading to additional uncertainties in the wind tunnel results. While a false adjustment of the propeller pitch angle would yield a consistent over- or underestimate of the simulated thrust, the scatter around the ideal values in Fig. 5b may be the result of uncertainties in the profile shapes. Nevertheless, no point violates the 10% tolerance band, which can be stated as sufficient for the preliminary analysis of aircraft propeller aerodynamics.

4.2 Overall propeller-wing-interaction model

To validate the overall propeller-wing-interaction model (PWIM), wing polars and spanwise lift distribution simulated with LIFTING_LINE are compared to TETRIS wind tunnel data. For the purpose of comparability, boundary conditions of model and test rig are aligned and calibration factors for the simulation results are introduced. First, the impact of the test rig's end plates are modeled within LIFTING_LINE by introducing a branching condition which couples the circulation at the wing tip with the circulation at the wing root. This avoids the typical loss of wing lift at the wing tip and approximates a nearly constant spanwise lift distribution as it can be expected from the end plates in the wind tunnel experiments. In addition, the evaluation of the wind tunnel experiments revealed a moderate lift slope of $C_{L\alpha} \approx 4.4$. This poor wing performance originates from the segment connections of the modular wing concept. To subtract the influence of these wing surface imperfections from the data comparison, the wing lift slope was corrected by a multiplication factor of $f_{C_{L\alpha}} = 4.4/2\pi = 0.7$ in LIFTING_LINE. Moreover, the findings by [10], where a propeller model using blade-element momentum theory approach in combination with LIFTING_LINE was investigated, yield a correction of the propeller-induced tangential velocities by a factor of 4. Pre-studies for multiple test configurations with XROTOR, however, showed that a correction factor of 1.4 for tangential propeller velocities is suitable to calibrate the model presented in this paper.

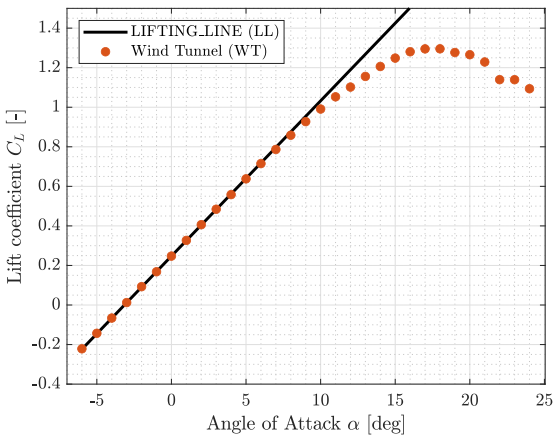

(a) Clean wing configuration

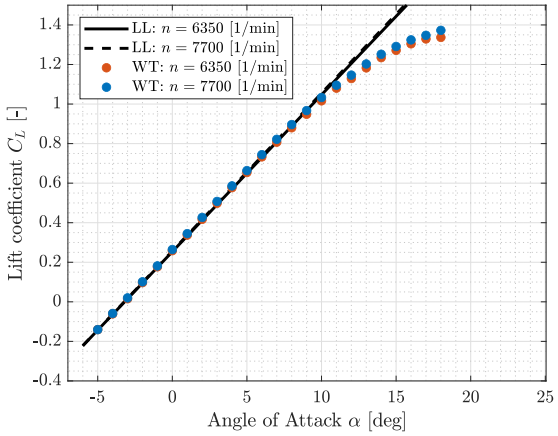

(b) Single motor configuration at $V = 16\ \mathrm{m\,s^{-1}}$ and $n = 6350, 7700\ \mathrm{min^{-1}}$

Figure 6 – Comparison of global aerodynamic results from LIFTING_LINE and wind tunnel data

Wing polars

In Fig. 6a, the results of the clean wing configuration are compared with wind tunnel data. Because LIFTING_LINE assumes non-viscous flow conditions, the stall region of the lift polar is not covered correctly by the analysis. Therefore, the results of the propeller-wing-interaction model are only valid for the linear part of the lift polar. However, the results in a range between $\alpha = -3°$ and $6°$ show good agreement with the measurement data when the presented lift slope calibration is applied. This is

specifically important for the correct interpretation of the following validation steps.

In Fig. 6b the results at a free stream velocity of $V = 16\,\mathrm{m\,s^{-1}}$ and varying rotational speeds of $n = 6350$ and $7700\ \mathrm{min^{-1}}$ are shown for the single motor configuration. Again, a good agreement between the aerodynamic model and the wind tunnel data is shown. The mean absolute deviation to the wind tunnel data is $\Delta C_L \approx 0.015$ at $n = 6350\ \mathrm{min^{-1}}$ and $\Delta C_L \approx 0.02$ at $n = 7700\ \mathrm{min^{-1}}$. Due to the presence of the propeller, the maximum lift coefficient is increased compared to the clean wing by $\Delta C_{Lmax} \approx 0.08$. Also, the wing lift slope was raised by 1.63% (@7700 $\mathrm{min^{-1}}$). Nevertheless, the overall impact of the varying rotational speeds can be stated as low for the isolated single motor configuration, which is particularly true for the linear part at low angles of attack. A more pronounced effect can be expected for a wing with mutiple propulsors.

Spanwise lift distribution

In Fig. 7 the results for the measured and simulated spanwise local lift at a free stream velocity of $V = 16\ \mathrm{m\,s^{-1}}$ and rotational speeds of $n = 6350$ and $7700\ \mathrm{min^{-1}}$ are shown. Herein, the spanwise position is expressed as the distance from the center line of the motor Δy normalized to the propeller radius R. Consequently, the spanwise positions $\Delta y/R = -1$ and $\Delta y/R = 1$ mark the non-contracted propeller blade length. The results demonstrate the typical lift distribution of propeller-wing-interactions, where the axial induced velocities lead to increased dynamic pressure and therefore to an increased wing lift. Whereas, depending on the rotational direction the tangential induced velocities lead to an increased or decreased effective wing angle of attack which results in an increased or decreased local wing lift, respectively.

The overall performance of the PWIM can be stated as satisfying for the intended purpose of preliminary aircraft analyses. Nonetheless, higher deviations occur at deviating angle of attacks from $\alpha = 0°$. One reason for this might be the results of the propeller model, which are based on the assumption of zero angle of attack. This leads to errors during the calculation of induced velocities at higher or lower angles of attack. Furthermore, higher deviations can be seen near the motor nacelle between $r/R = -0.5$ and $r/R = 0.5$, which might be result of the neglected nacelle effect. According to Veldhuis [14] the nacelle might lead to an increased axial velocity at the inner propeller radius. Due to the higher dynamic pressure, this would increase the resulting wing lift in this area as it is the case in the wind tunnel results.

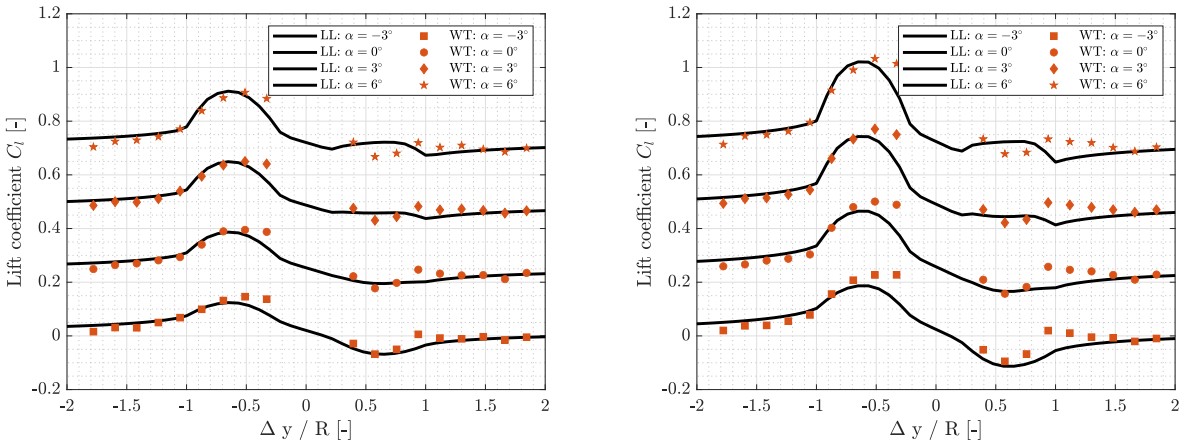

(a) Results at $n = 6350\ \mathrm{min^{-1}}$ and $V = 16\ \mathrm{m\,s^{-1}}$

(b) Results at $n = 7700\ \mathrm{min^{-1}}$ and $V = 16\ \mathrm{m\,s^{-1}}$

Figure 7 – Comparison of local spanwise lift results from LIFTING_LINE and wind tunnel data

5. Examples of Application

To demonstrate the use of the validated aerodynamic toolchain, it is integrated into a modular software framework for preliminary design of subscale test aircraft and resizing effects are studied. In

addition, the prospective use of the PWIM for wing load estimation is outlined. Both use cases are exemplified by the use of the aircraft layout definition *Wingfinity-BL* described in the following.

5.1 Preliminary Design of a Subscale Test Aircraft with Distributed Propulsion

Aircraft layout

The presented PWIM is applied to an ATR-42 like aircraft configuration. This aircraft configuration, called *Wingfinity-BL*, was derived during the LuFo V-3 project ELASTIK funded by the German government. The 3D layout is depicted in Fig. 8. The primary goal of ELASTIK is to develop advanced load estimation methods for future aircraft configurations. The aircraft configuration is characterized by six co-rotating distributed electrical propulsion systems (rotational direction to the wing tips) and a high aspect ratio wing ($\Lambda \approx 16$). It embodies a trade-off between current configurational trends that can be found in recent literature for regional aircraft concepts.

Figure 8 – Aircraft model *Wingfinity-BL*

SCALAR - Toolbox for preliminary design of subscale test aircraft

SCALAR combines classical conceptual design methods with the knowledge from the long-year expertise of the FST in design and construction of subscale test aircraft. A general overview of the software framework is given in Fig. 9. It follows a geometry-based aircraft design approach. Consequently, the external tool OpenVSP [15] is used for interactive specification of a reference geometry. Based on the results of a simple constraint and mission analysis (initial sizing), the specified geometry is scaled accordingly to match the determined initial design point (i.e. wing loading W/S and weight-to-power ratio W/P). From there, the assumed wing loading is examined in a full sizing iteration loop while W/P is fixed. To this end, conceptual-level analyses of aerodynamics, flight mechanics, structures, and systems are performed. This modular sizing process is executed until convergence of the aircraft size (i.e. wing loading W/S) is reached. So far, an aeroelastic analysis is not involved during this convergence loop. It will be addressed in future work. In the following, the impact of the enhanced PWIM compared to the sole use of LIFITNG_LINE (former implementation) as aerodynamic module of SCALAR on the sizing results for a STA model with distributed propulsion (*Wingfinity-BL*) is presented.

Sizing Results

The following sizing results are based on two different process settings. While the first setting contains the reference configuration with a sole use of LIFTING_LINE (PWIM disabled) during the aircraft sizing in SCALAR, the second setting contains the same aircraft configuration with the overall propeller-wing-interaction model presented in Sec. 2.

The results of the aircraft sizing are shown in Tab. 4. It can be seen, that the overall impact of the propeller-wing-interaction model on scaled model aircraft can be stated as of minor importance. Regarding the battery weight little to no improvement was achieved. Detailed analysis revealed that benefits regarding power consumption were mainly achieved during climb condition, whereas the cruise condition lead to a higher power consumption due to higher drag. In total, the mean power consumption was reduced by 0.5%. Nevertheless, the component based battery algorithm of SCALAR chooses the same battery type from the database of commercial-of-the-shelf (COTS)

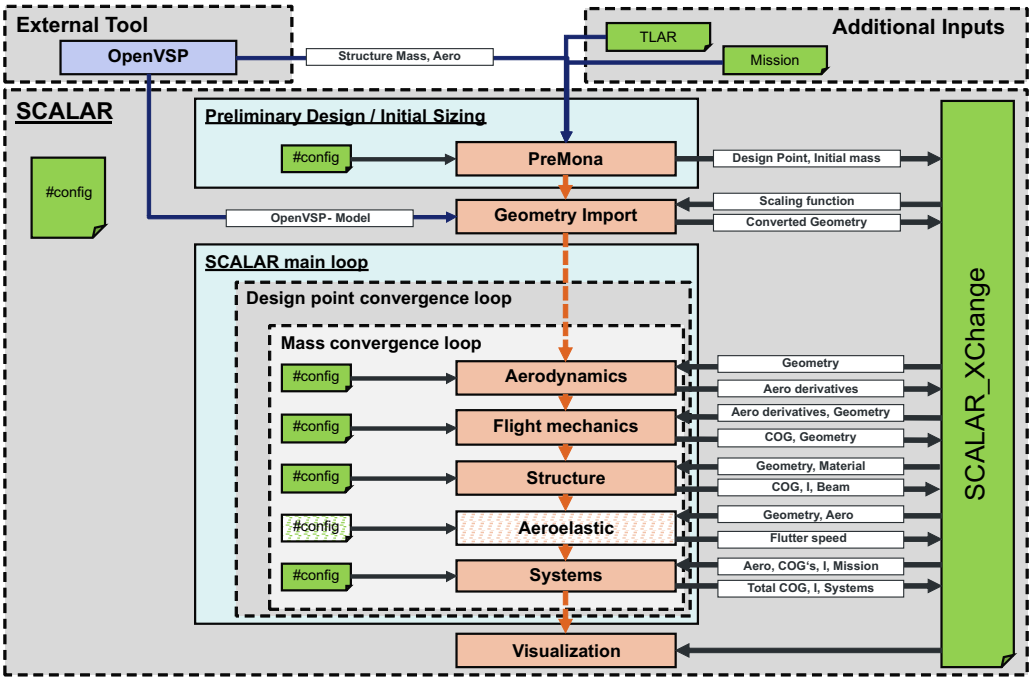

Figure 9 – Overview of the toolchain for the design and construction of subscale test aircraft (SCALAR)

system components, because the relative changes in simulated power consumption and peak power loads are comparatively small.
Higher impacts can be found regarding the total aircraft weight and reference wing area, which could be traced back to an advantageous lift distribution during the structure sizing. Due to the presence of the propeller slipstream the lift center is shifted inboard in direction of the fuselage (cf. Fig. 10b). This results in a reduced bending moment during the structure analysis of the wing beam. Since for all settings the wing beam is dimensioned to an ultimate load of $4.5g$, the beam is relived with increasing induced propeller velocities leading to smaller beam dimensions and a reduced structural weight.

Table 4 – Sizing results of *Wingfinity-BL* obtained with SCALAR

Propeller wing interaction model	Disabled	Enabled	Percentage Change
Structure weight [kg]	8.76	8.67	-1.03%
Systems weight (Battery) [kg]	10.03 (2.93)	10.03 (2.93)	0.00%
Payload weight [kg]	4.75	4.75	0.00%
Total weight [kg]	23.54	23.45	-0.38%
Reference wing area S_{ref} [m^2]	1.784	1.779	-0.28%
Mean power consumption [W]	640.5	636.2	-0.67%

5.2 Estimation of center of lift

As it was shown in Sec. 5.1, the introduction of the propeller-wing-interaction model leads to a detailed insight into the actual lift distribution of the wing. Depending on the current flight phase and propeller operating point, a variation of the center of lift can be observed. This variation with a sole use of LIFTING_LINE and with the overall propeller-wing-interaction model are compared in Fig. 10a based on the simple SCALAR mission analysis results. It can be seen that, by introducing propeller-wing-interactions the mean value of the center of lift was decreased from 44.87 percentage points to 43.98 percentage points. The variation range from minimum relative center of lift position to maximum relative position was increased from 2.50 percentage points ([44.30, 46.80]) to 10.18 percentage points ([35.79, 45.97]). In the context of the SCALAR toolchain, it was shown that in particular the decrease of the mean value of the center of lift, which mainly corresponds to the cruise condition, is relevant

for the aircraft sizing. The range of center of lift variation is of minor importance for the toolchain but emphasizes the importance of the propeller-wing-interaction model for further applications like aircraft health monitoring, loads estimation or load allevation. Particularly at flight conditions with high propeller impact (e.g. climb conditons) the analysis shows that a significant change in center of lift can be expected. This has to be accounted in the mentioned application examples since the center of lift directly correlates with the wing loads. Regarding this, the implemented aerodynamic toolchain and the corresponding detailed insight into the actual lift distribution provides encouraging results for further applications within the frame of ELASTIK.

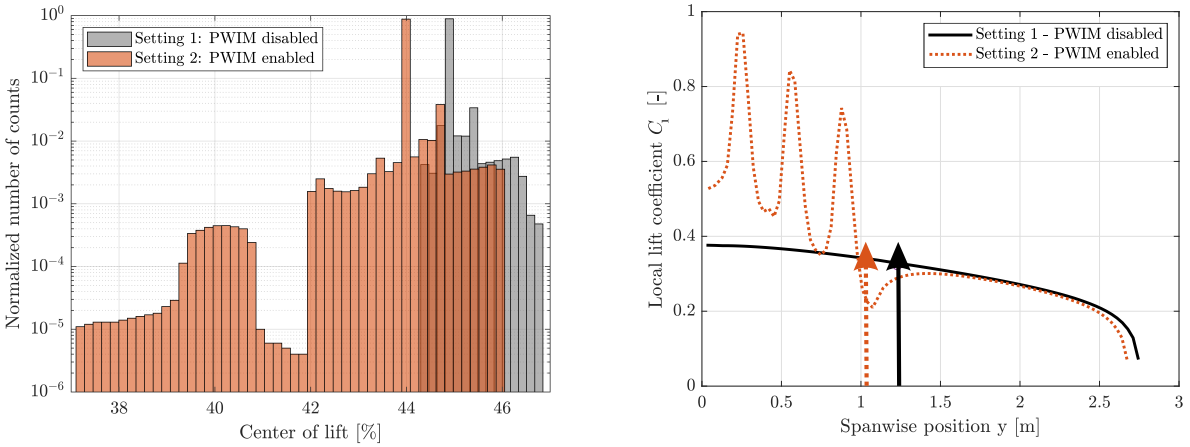

(a) Center of lift variation during flight mission

(b) Exemplary local lift at different PWIM settings

Figure 10 – SCALAR - flight mission results

6. Summary and outlook

In this publication a propeller wing interaction model based on the analysis programs XFOIL, XROTOR and LIFTING_LINE was integrated into a toolchain for preliminary design of subscale test aircraft (SCALAR). The extended toolchain is supposed to improve the analysis capabilities of aircraft with distributed propulsion during the aircraft design in SCALAR and for further applications by accounting the aerodynamic interaction between the propulsion system and the wing. The implemented method was compared to wind tunnel measurements at Hamburg University of Technology which revealed good agreement with less than 2.1% relative deviation between measured and simulated thrust of the propeller model for two different propellers. It was shown that the propeller wing interaction model is able to reproduce the wind tunnel results regarding wing polars and spanwise lift distribution. Nevertheless, to do so the tangential induced propeller velocities had to be corrected by a factor of 1.4 which underlines the complexity of modelling propeller slipstreams at low reynolds numbers and which still needs to be further addressed in future work. Subsequently, the extended toolchain was applied to the scaled model aircraft "'Wingfinity-BL"', which had been derived during the LuFo V-3 Project "'ELASTIK"'. The overall impact of the propeller-wing-interaction model on the results of the aircraft sizing can be stated as low. Mainly the structural weight was affected due to an advantageous lift distribution but this relation strongly depends on the rotational direction, propeller positioning and the flight phase. Despite the low impact on the aircraft design of subscale test aircraft the implemented aerodynamic toolchain gives a significant more detailed insight in the spanwise lift distribution and particularly the change of center of lift position during the flight mission. This can be an important basis for further applications like model based loads estimation methods.

7. Contact Author Email Address

mailto: oliver.luderer@tuhh.de, marc.juenemann@tuhh.de, frank.thielecke@tuhh.de

8. Copyright Statement

of any third party material included in this paper, to publish it as part of their paper. The authors confirm that they give permission, or have obtained permission from the copyright holder of this paper, for the publication and distribution of this paper as part of the ICAS proceedings or as individual off-prints from the proceedings.

9. Acknowledgement

The results of the presented paper are part of the work in the research project "'Advanced load analysis and observer methods for innovative aircraft configurations"' (ELASTIK), which is supported by the german Federal Ministry of Economic Affairs and Energy in the national LuFo V-3 program. Any opinions, findings and conclusions expressed in this document are those of the authors and do not necessarily reflect the views of the other project partners.

Gefördert durch:

Bundesministerium für Wirtschaft und Energie

aufgrund eines Beschlusses des Deutschen Bundestages

References

[1] A. Sobron. *On Subscale Flight Testing : Applications in Aircraft Conceptual Design*. Linköping University Electronic Press, 2018. DOI: 10.3384/lic.diva-152488.

[2] D. Raymer. *Aircraft design : a conceptual approach*. Reston, VA: American Institute of Aeronautics and Astronautics, 2012. ISBN: 9781600869112.

[3] M. Drela. "XFOIL: An Analysis and Design System for Low Reynolds Number Airfoils". In: *Lecture Notes in Engineering*. Springer Berlin Heidelberg, 1989, pp. 1–12. DOI: 10.1007/978-3-642-84010-4_1.

[4] M. Drela and H. Youngren. *XFoil*. URL: https://web.mit.edu/drela/Public/web/xfoil/.

[5] H. Himmelskamp, Aerodynamische Versuchsanstalt Göttingen, et al. *Profile Investigations on a Rotating Airscrew*. ARC-10856. Ministry of Aircraft Production, 1947. URL: https://books.google.de/books?id=VlK3tgAACAAJ.

[6] H. Snel, R. Houwink, et al. *Sectional Prediction of Lift Coefficients on Rotating Wind Turbine Blades in Stall*. ECN / C.: ECN. Netherlands Energy Research Foundation, 1994.

[7] Z. Du and M. Selig. "A 3-D stall-delay model for horizontal axis wind turbine performance prediction". In: *1998 ASME Wind Energy Symposium*. 1998. DOI: 10.2514/6.1998-21.

[8] R. MacNeill and D. Verstraete. "Blade element momentum theory extended to model low Reynolds number propeller performance". In: *The Aeronautical Journal* 121 (May 2017), pp. 1–23. DOI: 10.1017/aer.2017.32.

[9] M. Drela and H. Youngren. *XRotor*. URL: http://web.mit.edu/drela/Public/web/xrotor/.

[10] L. Lemke, O. Luderer, et al. "Aerodynamische Analyse verteilter Antriebe an einem Flügelsegment eines hochgestreckten Flügels". In: Deutscher Luft- und Raumfahrtkongress, 2019.

[11] H. Smelt R. und Davies. *Estimation of Increase in Lift Due to Slipstream*. Technical Report. 1937.

[12] M. Patterson, J. Derlaga, and N. Borer. "High-Lift Propeller System Configuration Selection for NASA's SCEPTOR Distributed Electric Propulsion Flight Demonstrator". In: *AIAA Aviation: 16th AIAA Aviation Technology, Integration, and Operations Conference*. 2016. ISBN: 978-1-62410-440-4. DOI: 10.2514/6.2016-3922.

[13] C. Liersch and T. Wunderlich. "A Fast Aerodynamic Tool for Preliminary Aircraft Design". In: *Multidisciplinary Analysis and Optimization Conference*. American Institute of Aeronautics and Astronautics, 2008. DOI: 10.2514/6.2008-5901. URL: https://doi.org/10.2514/6.2008-5901.

[14] L. Veldhuis. "Propeller Wing Aerodynamic Interference". Dissertation. Delft University of Technology, 2005. ISBN: 90-9019537-8.

[15] J. Gloudemans, P. Davis, and P. Gelhausen. "A rapid geometry modeler for conceptual aircraft". In: *34th Aerospace Sciences Meeting and Exhibit*. Reston, Virigina: American Institute of Aeronautics and Astronautics, 1151996. DOI: 10.2514/6.1996-52.